Article

Chinese Science Bulletin

Optoelectronics

November 2010 Vol.55 No.32: 3727–3733
doi: 10.1007/s11434-010-3195-3

A comprehensive consideration of bias voltage and temperature to extract the intrinsic frequency response of photodiodes

CHEN ShuoFu*, LI Liang, WU Hao, WANG LiXian, KE JianHong, LI Wei, XIE Liang & ZHU NingHua*

Institute of Semiconductors, Chinese Academy of Sciences, Beijing 100083, China

Received November 20, 2009; accepted February 8, 2010

Frequency response is one of the most important characteristics of photodiode (PD). The upper limitation of the bandwidth of a PD is determined by its intrinsic frequency response. Based on the extraction method to extract the intrinsic frequency response, we take a further study to analyze the impact of the reverse bias voltage and the temperature on the frequency response of PDs. With the help of physical model, the experimental data and fitted results based on the reverse bias voltage and temperature separately are discussed, then the most reliable intrinsic frequency response of a PD is obtained.

photodiode, intrinsic frequency response, extraction method, optoelectronic

Citation: Chen S F, Li L, Wu H, et al. A comprehensive consideration of bias voltage and temperature to extract the intrinsic frequency response of photodiodes. Chinese Sci Bull, 2010, 55: 3727–3733, doi: 10.1007/s11434-010-3195-3

The trend in optical communication systems towards higher transmission rates has led to the development of wide-bandwidth optical receivers. The bandwidth of a PD is determined by the response of extrinsic parasitic network and the intrinsic frequency response of the diode [1]. The mostly used fabricated PD actually contains package parasitic network, chip parasitic network and intrinsic photodiode [2,3]. The intrinsic frequency response offers the upper limitation of the bandwidth of a PD, since the effect of all the parasitic network can be eliminated by elaborate design.

To get the intrinsic frequency response of a PD, the response of cascaded network including a modulator, a photodiode and test fixtures is measured by vector network analyzer (VNA) in the conventional calibration method, and then the effect of the modulator and test fixtures is removed [4–6]. However, this method is much complicated, and the effect of parasitic parameter becomes obvious when the working frequency is increased. A simple method to extract the intrinsic frequency response was proposed based on the principle that the scattering parameters of parasitic network usually do not change with the bias voltage of photodiode [7]. However, the working temperature of a PD varies in practice use and has impact on the response characteristics, so the temperature factor should be taken into account when extracting the intrinsic frequency response.

Just as the bias voltage, the temperature does not affect the scattering parameters of the parasitic network, thus we take a further study on the extraction method considering both temperature and bias voltage factors. In this paper, the theory of the extraction method is briefly described, and then the impact of temperature and bias voltage on the drift velocity of carriers in the photodiode is analyzed. By subtracting and curve fitting the experimental data based on bias voltage and temperature separately, the results are obtained and discussed upon the definition of parameters and physical meaning. The best result is selected after the comparison, thus the intrinsic frequency response of PD and the physical parameters are finally obtained.

1 Theory of the extraction method

The current of a *p-i-n* PD involves four parts: the carrier

*Corresponding authors (email: sfchen@semi.ac.cn; nhzhu@semi.ac.cn)

© Science China Press and Springer-Verlag Berlin Heidelberg 2010

drift current, the carrier diffusion current, the displacement current and the dark current [1,8]. After a simplified yet realistic analysis [1,9,10], the *p-i-n* PD current is the sum of the dark current, the displacement current and photocurrent as given by

$$I_{pd} = I_{\text{dark}} + I_d + \frac{q}{W_i}(Nv_n + Pv_p), \tag{1}$$

where the dark current I_{dark} and the displacement current I_d have nothing to do with the optical signal. For an optical-input signal $P_{\text{in}} = P_0 + P_1 \exp(-jwt)$, where P_0 is the DC component of the optical power and P_1 is the AC component with angle frequency of ω. N and P are the numbers of electrons and holes in the i layer respectively. W_i is the width of the i layer, and is also the drift distance of the electron-hole pairs which are separated and accelerated in the opposite direction by the reverse electrical field. v_n and v_p are the velocities of electrons and holes, respectively. For InGaAs material, the drift velocities of electrons and holes vary with the temperature and the bias voltage [11,12], which would be described in the next section. v_n and v_p determine the drift times of electrons and holes by

$$\tau_n = \frac{kW_i}{v_n}, \tag{2}$$

$$\tau_p = \frac{(1-k)W_i}{v_p}, \tag{3}$$

where $0<k<1$ is a statistical coefficient that represents the position in the i layer where the electron-hole pairs originate.

After relative derivation [7], the intrinsic frequency response of the PD can be calculated by

$$H(w,T,V) = \frac{q\eta_0}{h\nu}\left(\frac{1}{\frac{1}{k}+iw\frac{W_i}{v_n}} + \frac{1}{\frac{1}{1-k}+iw\frac{W_i}{v_p}}\right). \tag{4}$$

This is the magnitude S_{21} parameter of the intrinsic PD.

The definitions of the scattering parameters of lasers and PDs are different from the electric network [13], written as

$$S^L = \begin{pmatrix} S_{11}^L & 0 \\ S_{21}^L & 0 \end{pmatrix}, \tag{5}$$

$$S^D = \begin{pmatrix} 0 & 0 \\ S_{21}^D & S_{22}^D \end{pmatrix}, \tag{6}$$

where the indicators L and D represent laser and PD respectively. The PD is constituted by two parts: the intrinsic PD is considered as a current source with a high resistance, and its S_{22} parameter is bias-independent when the applied reverse voltage is great enough. The scattering parameters of the photoelectric system including the laser and the intrinsic PD are given by

$$S^{LD} = \begin{pmatrix} S_{11}^L & 0 \\ S_{21}^L S_{21}^D & S_{22}^D \end{pmatrix}. \tag{7}$$

The whole network cascaded by the laser L, the intrinsic photodiode D and the extrinsic parasitic network P can be measured by the VNA, and the parameters S_{21} of the cascaded network can be expressed as

$$S_{21}^{LDP}(w,T,V) = \frac{S_{21}^L(w)S_{21}^D(w,T,V)S_{21}^P(w)}{1-S_{22}^D(w)S_{11}^P(w)}. \tag{8}$$

The two test ports of the calibrated network analyzer are SMA connectors. Therefore, the effects of the laser and the parasitic network cannot be eliminated from the measurement. However, by subtracting a certain response from the other responses (in decibels), the effects of the laser source, the parasitic network, the test fixture and other frequency variations that do not change with the bias voltage can be eliminated [13]. The response of PD at one bias level minus that at another bias level is given by

$$\begin{aligned} R(w) &= 10\log_{10}\left[\frac{S_{21}^{LDP}(w,T1,V1)}{S_{21}^{LDP}(w,T2,V2)}\right] \\ &= 10\log_{10}\left[\frac{S_{21}^{D}(w,T1,V1)}{S_{21}^{D}(w,T2,V2)}\right]. \end{aligned} \tag{9}$$

The measured responses can be curve-fitted to eq. (9) on a computer under the least squared method. The sum of squared errors between the calculated and measured values of the subtracted response can be minimized using a quasi-Newton method and a finite-difference gradient. Finally, we obtain the physical parameters and get the intrinsic response of the *p-i-n* PD.

2 The influence on the frequency response of the temperature and bias voltage

The InGaAs PIN PD is selected to analyze the influence on the frequency response of the temperature and bias voltage. The noise of the photodiode increases with the ascending temperature, which influences the receiving sensitivity of PD. The drift velocities of the carriers in the intrinsic layer vary with temperature [11,12], and decline with the decreasing temperature at a high electrical field. So the drift time becomes longer, which affects the frequency response characteristic of PIN PD [14,15], shown as the decrease of the bandwidth of 3 dB.

Windhorn et al. [11] described the relationship between the drift velocity of electron and the electrical field at different temperature, and depicted the effect of temperature on the electron saturation drift velocity. When the tempera-

ture increases, both the electron drift velocity and the saturation drift velocity decrease. The electron saturation drift velocity declines from 0.75×10^7 to 0.62×10^7 cm/s when the temperature increase from 95 to 300 K, but the electron drift velocity falls down faster than the electron saturation drift velocity. This literature did not express the variation of the electron drift velocity at different temperature and electrical fields.

Based on the empirical equations and the experimental results, Mohammad et al. [12] revised the expression of the drift velocity of the carriers, considering the influence of temperature. The revised equation is written as

$$v(E,\mu_{LF},a)=v_{CT}(E,\mu_{LF},1.0)+\left[v_p-v_{CT}(E,\mu_{LF},1.0)\right]\lambda_s, \tag{10}$$

where

$$\lambda_s=\exp\left\{-5.0\left[\left|\left(\frac{E_0}{E}\right)^a-1\right|\right]\right\}, \tag{11}$$

$$a=\left[\sigma\left(\frac{T}{T_0}\right)^2\right]. \tag{12}$$

T is the absolute temperature, T_0=300 K; v_p is the max measured drift velocity; σ is an adjustable parameter; E is the electric field intensity, E_0 is the value of E when the drift velocity reaches v_p; for InGaAs material, σ=0.23, E_0=4.1 kV/cm, v_p=3.1×10^7 cm/s; v_{cT} is the same one in [11]

$$v_{CT}(E,\mu_{LF},\alpha)=v_{HF}E=\frac{\mu_{LF}E}{\left[1+\left(\frac{\mu_{LF}E}{v_s}\right)^{\alpha}\right]^{\frac{1}{\alpha}}}, \tag{13}$$

where μ_{LF} is the low-field mobility of the carriers. For InGaAs material, the μ_{LF} of the electron is 1.05×10^4 cm^2/V s and μ_{LF} of the hole is 420 cm^2/V s.

By substitution the eqs. (11)–(13) to eq. (10), the drift velocity of the carriers is expressed as

$$v(V,T)=\frac{\mu E}{1+\frac{\mu E}{v_s}}+\left(v_p-\frac{\mu E_0}{1+\frac{\mu E_0}{v_s}}\right)\exp\left[-5.0\left|\left(\frac{E_0}{E}\right)^{\sigma\left(\frac{T}{T_0}\right)^2}-1\right|\right]. \tag{14}$$

By utilizing eq. (14), the calculated electron drift velocity in the InGaAs intrinsic region is shown in Figure 1, which is consistent with the measured results in [11].

According to [1], another set of equations also agrees well with experimental data:

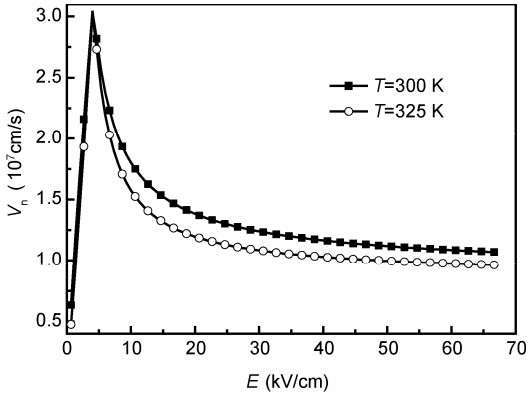


Figure 1 The calculated drift velocity vs E for electron in InGaAs at 300 and 325 K.

$$v_n(E)=\frac{\mu_n E+\beta V_{nL}E^r}{1+\beta E^r}, \tag{15}$$

$$v_p(E)=V_{pL}\tanh\left(\frac{\mu_p E}{V_{pL}}\right), \tag{16}$$

where μ_n and μ_p are the motilities of electrons and holes, V_{nL} and V_{pL} are high field velocities of electrons and holes, respectively, β and r are adjustable parameters, and E is the reverse electrical field as given by $E=(V_j-V_{bj})/W_i$, where V_{bj} is the space-charge drop, and V_j is the external reverse bias voltage.

The calculated relationship of electron drift velocity and the bias voltage by eq. (15) is consistence with that by eq. (14). However, it is different to calculate the hole drift velocity when using the two equations above. As shown in Figure 2, the upper curve is calculated by eq. (16), and the lower curve is calculated by eq. (14). The upper curve shows that the hole drift velocity increases quickly at the beginning, and then keeps invariant when the electrical field is above 30 kV/cm, while the lower curve shows that the hole drift velocity keeps increasing before the electrical field achieves

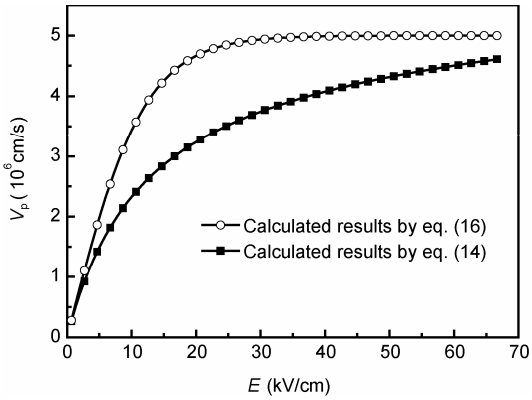


Figure 2 The drift velocity *vs* E plot for holes in InGaAs calculated by eqs. (14) and (16).

Samsung Exhibit 1043, Page 3 of 7

70 kV/cm. Therefore, the fitting results can be quite different when utilizing these two sets of equations.

3 Experimental results

3.1 The extraction method based on bias voltage

The system setup is shown in Figure 3, including a VNA, a DFB laser, a coplanar microwave probe and an optical coupling system. The PD under test is a high-speed InGaAs *p-i-n* PD with coplanar electrodes from Opto Speed. The lighwave source used in our experiment contains a DFB laser module and a 40-GHz $LiNbO_3$ optical waveguide modulator from CODEON Inc. An HP8720D VNA is used to measure the frequency response of the PD chip by an on-wafer coplanar strip microwave probe ACP40-GS-200 from Cascade Microtech Inc. The VNA is calibrated to two coaxial ports with a full two-port calibration. The probe is considered as a part of the parasitic network, and its effects can be removed in the subtraction procedures.

Figure 4 gives the measured frequency response at different reverse bias voltage. The response is not flat, since the effects of parasitic network and probe are included in the measurement. It is also obvious that the frequency response is higher and the 3 dB bandwidth becomes wider when the bias voltage is increasing.

For convenience, we subtract the response at a lower bias voltage from that at a higher bias voltage. Since the relationship between the drift velocity of the carriers and the bias voltage can be described in different equations, the fitting results using the same experimental data must be different. Figure 5 shows the fitting results calculated by eqs. (15) and (16). Table 1 gives the extracted values of the physical parameters of the PD. Figure 6 shows the fitting results calculated by eq. (14). Table 2 gives the extracted values of the physical parameters of the PD.

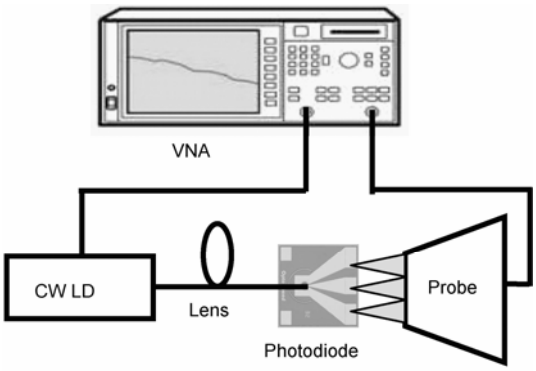


Figure 3 The system setup to measure frequency response of the photodiode chip.

Table 1 Parameter values obtained by Fitting 1

Parameter	Value
W_i (μm)	1.45
k	0.245
μ_n (cm^2/V s)	1050
μ_p (cm^2/V s)	420
V_{nL} (cm/s)	8×10^6
V_{pL} (cm/s)	5×10^6
β	7.4×10^{-10}
r	2.5

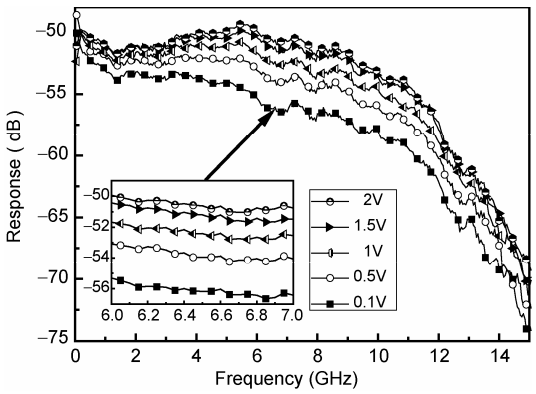


Figure 4 The frequency response of photodiode at different bias voltages.

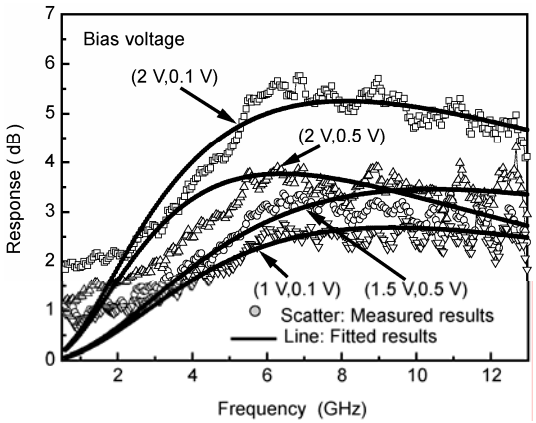


Figure 5 Measured and fitted results for the subtracted frequency response by eqs. (15) and (16).

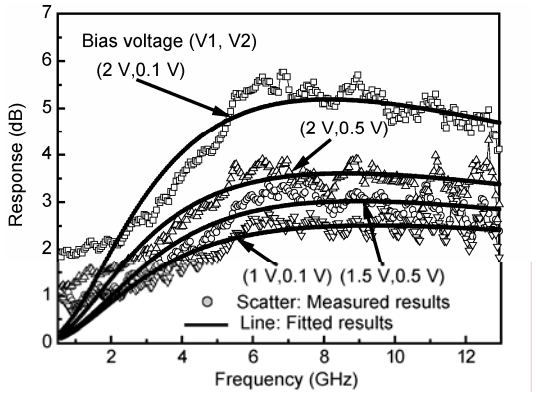


Figure 6 Measured and fitted results for the subtracted frequency response by eq. (14).

Table 2 Parameter values obtained by Fitting 2

Parameter	Value
W_i (μm)	1.27
k	0.137
μ_n (cm^2/V s)	1050
μ_p (cm^2/V s)	420
V_{nL} (cm/s)	8×10^6
V_{pL} (cm/s)	4.85×10^6
E_0 (kV/cm)	4.1
V_{nl} (cm/s)	3.1×10^7

3.2 The extraction method based on temperature and bias voltage

After the measurement of frequency response at different bias voltages, the temperature control system is added into the test system to measure the frequency response of PD at different temperature.

With the reverse voltage biased at 0.28, 0.85, 1.8 V, we measure the frequency response of PD at 10, 25, 35, 45, 50°C separately. Figure 7 shows the frequency response at different temperature and biased at 1.8 V, which shows that the frequency response decreases with the incremental temperature.

The relationship between the measured 3 dB bandwidth and the temperature at different bias voltage is shown in Figure 8. The bandwidth declines with the increasing temperature when biased at the same voltage, while the bandwidth can increase sharply when adding the reverse bias voltage at the same temperature.

Figure 9 shows the subtracted frequency response of the PD at different temperature when the reverse voltage biased at 1.8 V. It is obvious to see that the curve of 323 K subtracting from 283 K is the highest and the curve of 323 K subtracting from 308 K is the lowest. Their difference is less than 1 dB and is proportional to the range of the temperature. When fixing the bias voltage and only changing the temperature, the difference of frequency response of the PD is very small. It means that the temperature factor has relative less influence on the frequency response of PD. The amplitude jitters of frequency response in Figure 9 might be caused by our self-made temperature control system which is not stable when its working temperature is set too high or too low.

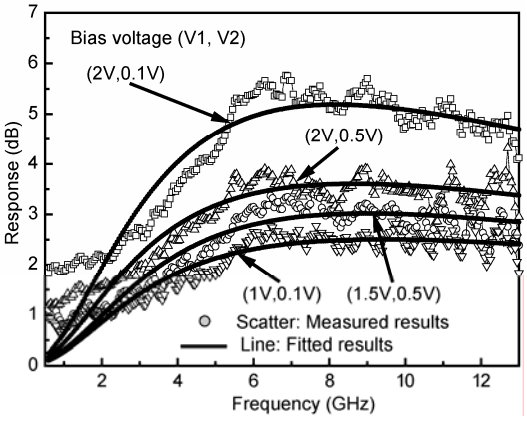


Figure 7 Measured frequency response at different temperature when the reverse bias voltage is 1.8 V.

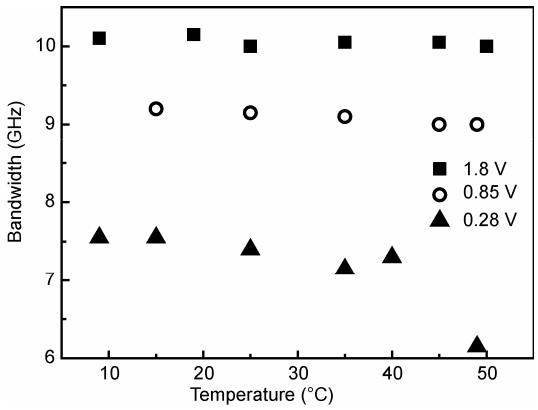


Figure 8 Measured 3 dB bandwidth *vs T* at different bias voltage.

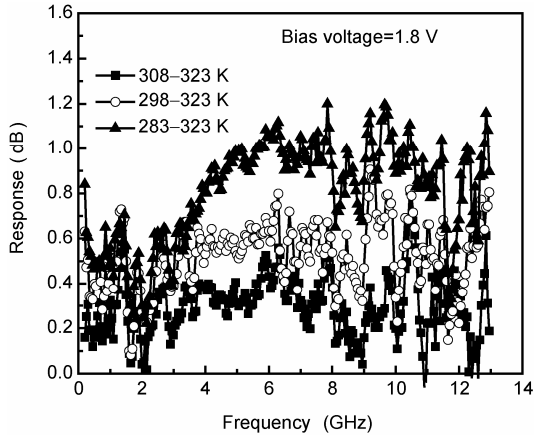


Figure 9 Measured subtracted frequency response at different temperature when the reverse bias voltage is 1.8 V.

Since the temperature effect is not obvious to the response of PD, we have to take into account the interaction of different temperature and different bias voltage to extract the intrinsic frequency response of the PD. We choose four sets of experimental conditions, and the reverse bias voltage and the temperature are set at 1.8 V 10°C, 0.28 V 50°C, 1.8 V 20°C and 0.28 V 35°C in sequence. Then we subtract the results between 1.8 V 10°C and 0.28 V 50°C, and that between 1.8 V 20°C and 0.28 V 35°C. Figure 10 shows the fitting results calculated by eq. (14). Table 3 gives the extracted values of the physical parameters of PD.

3.3 Analysis and comparison

The parameters such as the width of the absorption region W_i and the position parameter k have relatively high impact on the frequency response. Yet other parameters such as the

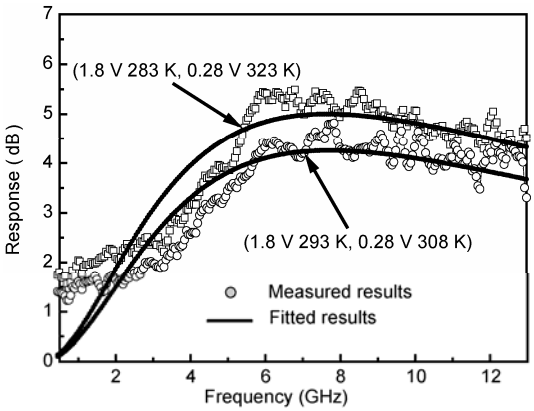


Figure 10 Measured and fitted frequency response at different temperature and bias voltages.

Table 3 Parameter values obtained by Fitting 3

Parameter	Value
W_i (μm)	1.172
k	0.157
μ_n (cm^2/V s)	1050
μ_p (cm^2/V s)	420
V_{nL} (cm/s)	8×10^6
V_{pL} (cm/s)	4.85×10^6
E_0 (kV/cm)	4.1
V_{nl} (cm/s)	3.1×10^7

saturation drift velocity are not important since they are the internal parameters belonging to the material itself, and are almost unchanged with the temperature and the bias voltage. For these less relevant parameters, we can select reasonable values and make them fixed in the fitting process. Table 4 gives the key parameters W_i and k obtained from the three fitting methods.

k indicates the position of the incident light. If the value of k is smaller, the incident position would be closer to the N region. Thus, the fitting results show that the photodiode is an N region incident type PD, which agrees with the facts. Also k reflects the original position of the photo-induced electrons and holes. The k should meet the equation: $\exp(-\alpha\times k\times W_i)=0.5$ because k is the center position of the photo-induced carriers, thus the calculated product of $k\times W_i$ is about 0.35. Then we compare the three fitting results, and find that the first method is reasonable. Therefore, the intrinsic frequency response of the *p-i-n* PD based on the first fitting method is drawn in Figure 11.

Table 4 Comparison of three fitting results

Fitting type	W_i (μm)	k
Fitting 1 based on bias voltage (eqs. (19) and (20))	1.45	0.245
Fitting 2 based on bias voltage (eq. (18))	1.27	0.137
Fitting 3 based on bias voltage and temperature (eq. (18))	1.172	0.157

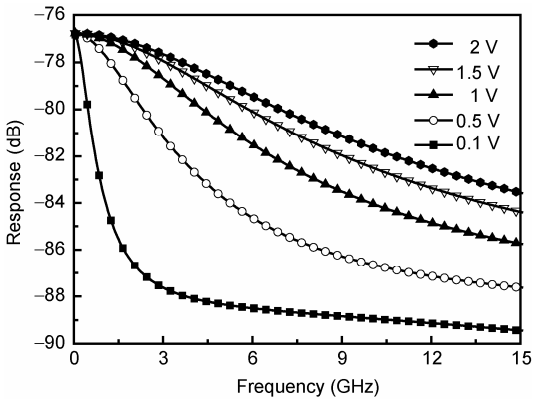


Figure 11 Calculated intrinsic frequency response of the *p-i-n* PD.

4 Conclusions

The extraction method is a simple method to extract the intrinsic frequency response of PD. This paper performs three fitting processes based on the bias voltage and the temperature separately. However, it is not convenient to use the temperature box to control the temperature since the PD chip is placed on the probe test station; in addition, the probe is not suitable to work at high temperature, therefore the range of temperature is so limited that the results are not good when considering the factor of temperature.

The significance to analyze the intrinsic frequency response is listed as follows:

(i) The upper limitation of the PD can be obtained.

(ii) The extraction method supplies a simple way to characterize the physical parameters of the active layer materials.

(iii) The parasitic parameters of the package network and the chip can be obtained by comparing with the results of packaged PD, and then with the equivalent circuit model of the whole PD can be established, consequently the comprehensive optimum design of the PD chip and its microwave packaging can be proceeded [16,17].

Moreover, the comprehensive extraction method can be further applied to other PDs that differ from the common *p-i-n* PDs, such as avalanche PDs, waveguide PDs, metal-semiconductor-metal PDs, etc.

This work was supported by the National Natural Science Foundation of China (60820106004, 60536010, 60777029 and 60837001), National Program on Key Basic Research Program of China (G2006CB604902 and G2006CB302806), National High Technology Research and Development Program of China (2009AA03Z409) and Major International Cooperation Projects of China (2006dfa11880).

1 Dentan M, Cremoux B D. Numerical simulation of the nonlinear response of a p-i-n photodiode under high illumination. J Lightwave Technol, 1990, 8: 1137–1144

2 Kimukin I, Biyikli N, Butun B, et al. InGaAs-based high-performance p-i-n photodiodes. IEEE Photon Technol Lett, 2002, 14:

366–368
3 Kato K, Hata S, Kawano K, et al. Design of ultrawide-band high sensitivity p-i-n photodetectors. IEICE Trans Electron, 1993, E76-C: 214–221
4 Debie P, Martens L, Kaiser D. Improved error correction technique for on-wafer lightwave measurements of photodetectors. IEEE Photon Technol Lett, 1995, 7: 418–420
5 Hale P D, Clement T S, Williams D F, et al. Measuring the frequency response of gigabit chip photodiodes. J Lightwave Technol, 2001, 19: 1333–1339
6 Zhu N H, Liu Y, Pun E Y, et al. Scattering-parameter measurement of laser diodes. Opt Quantum Electron, 2002, 34: 747–757
7 Huang H P, Zhu N H, Liu Y. Extraction of intrinsic frequency response of p-i-n photodiodes. IEEE Photon Technol Lett, 2005, 17: 2155–2157
8 Chen W Y, Yang S R, Liu S Y. Optoelectronic Devices Circuit Model and the Circuit-Level Simulation of OEIC (in Chinese). Beijing: National Defense Industry Press, 2001
9 Lucovski G, Schwarz R F, Emmons R B. Transit-time considerations in p-i-n diodes. J Appl Phys, 1964, 35: 622–628
10 Sano E, Yoneyama M. Mixed photonic/electronic circuit simulation including transient noise sources. IEICE Trans Electron, 1995, E78-C: 447–453
11 Windhorn T H, Cook L W, Stillman G E. Temperature dependent electron velocity-field characteristics for $In_{0.53}Ga_{0.47}As$ at high electric fields. J Electron Mater, 1982, 11: 1065–1082
12 Mohammad S N. Unified model for drift velocities of electrons and holes in semiconductors as a function of temperature and electric field. Solid State Electron, 1992, 35: 1391–1396
13 Hale P D, William D F. Calibrated measurement of optoelectronic frequency response. IEEE Trans Microw Theory Tech, 2003, 51: 1422–1429
14 Yoshino K, Muramoto Y, Furuta T, et al. High-speed uni-travelling-carrier photodiode module for ultra-low temperature operation. Electron Lett, 2005, 41: 1030–1031
15 Jun D H, Jang J H, Song J I. Effect of temperature on bandwidth and responsivity of uni-traveling carrier and modified uni-traveling carrier photodiodes. Jpn J App Phys, 2007, 46: 2360–2363
16 Liu Y, Chen S F, Wang X, et al. Overall optimization of high-speed semiconductor laser module. Chinese Sci Bull, 2009, 54: 3697–3703
17 Gao J J. High frequency modeling for quantum-well laser diodes. Chinese Sci Bull, 2009, 54: 3633–3638

Samsung Exhibit 1043, Page 7 of 7